

# Snow Avalanche Frequency Estimation (SAFE): 32 years of monitoring remote avalanche depositional zones in high mountains of Afghanistan

Arnaud Caiserman<sup>1\*</sup>, Roy C. Sidle<sup>1</sup>, Deo Raj Gurung<sup>2</sup>

<sup>1</sup> Mountain Societies Research Institute – University of Central Asia, Khorog, 736000, Tajikistan

A. Caiserman ORCID: <https://orcid.org/0000-0003-4580-6633> ; corresponding author: [arnaud.caiserman@ucentralasia.org](mailto:arnaud.caiserman@ucentralasia.org)

Roy C. Sidle ORCID: <https://orcid.org/0000-0002-5004-4154>

<sup>2</sup> Aga Khan Agency of Habitat, Dushanbe, 734013, Tajikistan

*Correspondence to:* Arnaud Caiserman ([arnaud.caiserman@ucentralasia.org](mailto:arnaud.caiserman@ucentralasia.org))

**Abstract.** Snow avalanches are the predominant hazards in winter in high elevation mountains. They cause damage to both humans and assets but cannot be accurately predicted. Until now, only local maps to estimate snow avalanche risk have been produced. Here we show how remote sensing can accurately inventory large avalanches depositional zones every year in a large basin using a 32-yr snow index derived from Landsat satellite archives. This Snow Avalanche Frequency Estimation (SAFE) built in an open-access Google Engine script maps snow hazard frequency and targets vulnerable areas in remote regions of Afghanistan, one of the most data-limited areas worldwide. SAFE correctly detected of the actual depositional zones of avalanches identified on Google Earth and in the field (Probability of Detection 0.77 and Positive Predictive Value 0.96). A total of 810,000 large depositional zones of avalanches occurred since 1990 within an area of 28,500 km<sup>2</sup> with a mean frequency of 0.88 avalanches<sup>km<sup>2</sup>-1</sup>, damaging villages and blocking roads and streams. Snow avalanche frequency did not significantly change with time, but a northeast shift of these hazards was evident. SAFE is the first robust model that can be used worldwide and is especially capable of filling data voids on snow avalanche impacts in inaccessible regions.

## 1. Introduction

Snow avalanches are among the fastest, up to 61 ms<sup>-1</sup>, and therefore most dangerous natural hazards in mountain areas (Louge et al., 2012). Casualties associated with avalanches are numerous; in 2021 alone, 37 fatalities occurred in the US (Colorado Avalanche Information Center, 2021) and 127 in Europe (European Avalanches Warning Services, 2021), but avalanche monitoring is not consistent across the globe. Most remote mountain regions and communities are not systematically monitored for avalanche occurrence. Avalanche surveys amongst remote villages are sparse because regions are uninhabited; however, avalanches can block connecting roads every year since avalanche volumes range from hundreds to several tens of thousand cubic meters (Gubler, 1987). Where weather stations exist, avalanches can be predicted based on snow depth and other weather parameters (Greene et al., 2016). However, the global weather monitoring of mountainous areas is scattered and very sparse in developing nations.

34 To support these science and government priorities in remote mountain regions, it is necessary to introduce a user-  
35 friendly, open-access method that maps snow avalanches on an annual basis across wide areas where internet  
36 connection and monitoring systems are not always available. As an example, half of the land surface of  
37 Afghanistan is above 2000 m a.s.l. and 80% is mountainous (Asad Sarwar, 2002). Among Central Asian nations,  
38 Afghanistan's population is most at risk of avalanche hazards; 22,477 inhabitants at risk compared to 5183 in  
39 Tajikistan (Chabot and Kaba, 2016). Particularly, northeast Afghanistan (Badakhshan) is one of the most  
40 vulnerable regions, especially from December through March (Mohanty et al., 2019). Several international  
41 initiatives have been implemented in Afghanistan to forecast avalanches or assess their risks on local communities.  
42 According to USAID, 30,600 buildings are at risk of avalanches in Badakhshan based on daily snow depth  
43 measurements (USAID, 2021). The Aga Khan Agency for Habitat (AKAH) collects snow depth data and uses  
44 models such as Alpine3D and SNOWPACK to forecast avalanche prone regions in Tajikistan, Afghanistan, and  
45 Pakistan (Bair et al., 2020). Other products have been developed, such as avalanche susceptibility and exposure  
46 maps (Kravtsova, 1990; World Bank, 2017). Another approach is to combine topographic maps and snow data via  
47 the RAMMS:AVA models (GFDRR, 2018), but these are not open access. Finally, it is possible to count the  
48 number of avalanches in each district as done by the United Nations in their map *Districts Affected by Avalanches*  
49 (OCHA-United Nations, 2012), but this is time consuming and may miss some events across large areas.

50  
51 Detecting the avalanches is a challenge and requires temporal as well as spatial data, especially for large areas.  
52 Remote sensing technology, both air and spaceborne, can cover large areas at different times of the year. Indeed,  
53 the frequent collection of satellite images over the same area enables the detection of changes in snow cover as  
54 well as other hazards, such as floods and landslides. Until recently, the use of remote sensing in avalanche detection  
55 was sparse due to low resolution, and the automation of such processes was even more difficult because of the  
56 lack of relevant algorithms that can compute big data (Eckerstorfer et al., 2016). Other remote sensing approaches  
57 for avalanche detection have used radar, Lidar, and optical data. Radar satellites, such as Sentinel-1A and B, are  
58 now commonly used for detecting mass movements by assessing backscatter signal changes between two time  
59 periods (before and after movement) by a co-registration of the two images. Backscatter values provide  
60 information on terrain roughness and any change indicates that a mass movement or a significant erosion event  
61 occurred in a given area. **Vickers et al. (2016) conducted one of the first studies utilizing Sentinel-1 products to  
62 detect avalanches debris by developing an unsupervised classification.** This technology seems very promising for  
63 avalanche detection (Eckerstorfer et al., 2017; Malnes et al., 2015; Martinez-Vazquez and Fortuny-Guasch, 2008;  
64 Schaffhauser et al., 2008; Tompkin and Leinss, 2021; Yang et al., 2020). **Using TerraSAR-X and Sentinel-1  
65 products, Leinss et al. (2020) mapped avalanches, demonstrating the potential of radar products in snow hazard  
66 detection.** However, the acquisition of frequent radar images is too recent to use this technique to detect historical

67 avalanches. In addition to optical, radar or Lidar data, other studies used Digital Elevation Models (DEMs) and  
68 topographic parameters to determine the influence of terrain on avalanches in Switzerland (Maggioni and Gruber,  
69 2009). Other studies incorporated other parameters such as morphology and vegetation to define potential  
70 avalanche zones and ran the Avalanche Flow and Run-out Algorithm to automatically detect potentially affected  
71 regions by avalanches (Barbolini et al., 2011). Moreover, the combination of snow measurements (depth) and high  
72 resolution DEMs have proved useful in snow hazard detection (Bühler et al., 2018a) Lidar is being used in the  
73 same regard with a higher level of precision. Lidar sensors measure snow depth before and after events at submeter  
74 resolutions (Prokop, 2008; Deems et al., 2013; Prokop et al., 2013; Hammond et al., 2018). However, this  
75 technology remains very expensive, and the spatial coverage is limited. Therefore, Lidar data are not suitable for  
76 avalanche detection at the basin scale. In addition to Optical, Radar or Lidar data, other studies used Digital  
77 Elevation Models and topographic parameters to determine the terrain influence on avalanches in Switzerland  
78 (Maggioni and Gruber, 2009). Some other studies added other parameters such as morphology and vegetation to  
79 define potential avalanche zones and ran Avalanche Flow and Run-out Algorithm to automatically potentially  
80 affected regions by avalanches (Barbolini et al., 2011). Moreover, the combination of snow measurements (depth)  
81 and high resolution DEMs proved its efficiency in snow hazards detection (Bühler et al., 2018a).

82 Optical data are the most available data in terms of spatial and temporal resolution as well as historical archives.  
83 Thus, we used optical data to detect avalanches on a long-term basis. Landsat-5, 7 and 8 products were used as  
84 their resolution (30 m, 900 m<sup>2</sup>) is sufficient to detect small avalanches (Eckerstorfer et al., 2016). Most of these  
85 data are available at a global scale. Optical sensors can detect areas covered or not covered by snow and this  
86 approach has been used in multiple studies during the past decade. Manual approaches or indices have been used  
87 in such studies. For example, Landsat-8 Panchromatic images (15 m) in combination with radar images were used  
88 to detect avalanches in Norway (Eckerstorfer et al., 2014). Such combinations were also recently used in west  
89 Greenland to map a large number of avalanches after an unprecedented snow event (Abermann et al., 2019). To  
90 our knowledge, only one recent study automated the detection of avalanches using remote sensing products and  
91 an open-access scripting approach (Smith et al., 2020). This study downloaded avalanches annually for a given  
92 region of interest using available Landsat-8 images and computed NDSI for each image. NDSI differentiated so  
93 called 'supraglacial debris' from snow cover, for the date of interest. However, this approach only covers high  
94 elevations areas while our study aims to detect avalanches proximate to local communities at lower elevations  
95 (typically valleys). Manual and visual approaches, despite the time consuming process, can also be applied to  
96 detect avalanches using high resolution images (e.g., SPOT-6), mid-resolution (e.g., Sentinel-2A and B images),  
97 or even Google Earth images (Singh et al., 2020; Yariyan et al., 2020; Hafner et al., 2021). Across a wide area  
98 (12,500 km<sup>2</sup>) individual snow avalanches were manually digitized using high resolution SPOT-6 images (Bühler  
99 et al., 2019). Terrain parameters like slope gradient and curvature have also been added to the avalanche detection

100 process using DEMs combined with Landsat-8 images (Bühler et al., 2018b; Singh et al., 2019). Integrated criteria  
101 are therefore recommended to detect avalanches. To our knowledge, no long-term avalanches mapping studies  
102 using remote sensing have been conducted in the world, especially not in Afghanistan.

103

104 The general objective of this study is to map annual **depositional** zones of avalanche occurrence over the past 32  
105 years using Landsat image archives in Badakhshan region, Afghanistan. Such long-term monitoring is the first  
106 attempt globally and enables us to map the frequency of **depositional** zones of avalanches that impact valley  
107 communities. Thus, we used optical data to detect **depositional** zones on a long-term basis and built an open-access  
108 script in Google Engine interface: *Snow Avalanche Frequency Estimation (SAFE)*. Landsat-5, 7 and 8 products  
109 were used as their resolution (30 m, i.e., minimum detectible size of 900 m<sup>2</sup>) is sufficient to detect larger avalanches  
110 (Abermann et al., 2019; Eckerstorfer et al., 2016, 2014; Hafner et al., 2021; Singh et al., 2019, 2020; Smith et al.,  
111 2020; Yariyan et al., 2020). Our objective is to automatically map annual **depositional** zones of avalanche  
112 occurrence over the past 32 years using Landsat-5, 7 and 8 image archives in the Amu Panj basin of Afghanistan.  
113 **SAFE is applicable in any high mountains of the world, such as Tien Shen, Himalaya, Hindu Kush, Karakoram or**  
114 **Andes, but not restricted to these, where snow avalanches deposits can be detected every year by satellite images**  
115 **for a long time before completely melting.** These outputs are of keen interest to decision makers who can use this  
116 automated process to map avalanche hazard in the future. The most vulnerable areas, villages and roads, were  
117 mapped for improve future planning. In addition, this research enables the monitoring of **depositional** zones of  
118 avalanche evolution over the past 32 years. Such analyses should strengthen local community resilience to snow  
119 avalanches.

120

## 121 **2. Materials and methods**

### 122 *2.1 Study area*

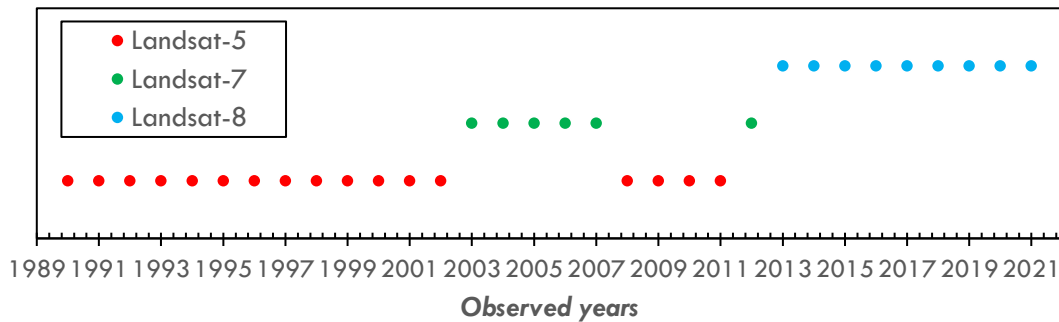
123 The study covers the most mountainous region of Afghanistan – Badakhshan in the Amu Panj basin located in the  
124 northeast portion of the country. Average elevation is 2761 m and mean slope gradient is 21%. This region spans  
125 from Bamyan Province to the Hindu Kush range, up through the Wakhan corridor in the far east of Afghanistan.  
126 The summit is Nowshak Peak at an elevation of 7492 m a.s.l. The western part of Amu Panj basin is rather flat  
127 and not prone to avalanches. Annual precipitation is about 600 mm occurring mostly as snow between February  
128 and May (Zhang et al., 2015). This terrain and precipitation characteristics lend Badakhshan very prone to  
129 avalanches. The basin is large (28,580 km<sup>2</sup>), justifying automated avalanche detection to cover this area in a  
130 reasonable amount of time using Google Engine. Despite the remoteness of this region, Badakhshan has a  
131 population of 950,953 inhabitants (Islamic Republic of Afghanistan Governmental Website, 2021) distributed in

132 4154 villages, mainly in valleys. However, 35% of the villages in Badakhshan are located at elevations above 2000  
133 m, increasing the vulnerability of these communities to avalanches.

134

### 135 2.2 Landsat archives for snowpack analysis

136 This analysis requires the integration of numerous data into a Google Engine Java script. Firstly, a mosaic of  
137 different Landsat images is created every year in the Amu Panj basin. Depending on the year of interest, Landsat-  
138 5 ([https://developers.google.com/earth-engine/datasets/catalog/LANDSAT\\_LT05\\_C01\\_T1\\_SR](https://developers.google.com/earth-engine/datasets/catalog/LANDSAT_LT05_C01_T1_SR)), Landsat-7  
139 ([https://developers.google.com/earth-engine/datasets/catalog/LANDSAT\\_LE07\\_C01\\_T1\\_SR](https://developers.google.com/earth-engine/datasets/catalog/LANDSAT_LE07_C01_T1_SR)), or Landsat-8  
140 ([https://developers.google.com/earth-engine/datasets/catalog/LANDSAT\\_LC08\\_C01\\_T1\\_SR](https://developers.google.com/earth-engine/datasets/catalog/LANDSAT_LC08_C01_T1_SR)) images were  
141 downloaded. Within a given year the same satellite images were used. Before 1990, coverage by Landsat-5 was  
142 insufficient in this region of Afghanistan. Landsat images were directly downloaded from Google Engine Archives  
143 under their *ImageCollection*. Depending on the availability of images and the year of interest, one satellite or  
144 another was used (Figure 1).



145

146 **Figure 1. Landsat archives used for **depositional** zones of avalanches detection since 1990.**

147

### 148 2.3 Shuttle Radar Topography Mission-30 for terrain selection

149 Detecting **avalanche deposits** requires terrain parameters defined by using the Shuttle Radar Topography Mission-  
150 30 (<https://dwtkns.com/srtm30m/>). This Digital Elevation Model was collected in 2000 and is globally available  
151 on the United States Geological Survey data portal at a spatial resolution of 30 m. SRTM-30 is used in this study  
152 to delineate the regions of interest by deriving stream channels from the DEM.

153

### 154 2.4 Terra MODIS MOD10A2.006 for snow line analysis

155 The ROI (regions of interest) are delineated using Terra MODIS MOD10A2.006  
156 (<https://nsidc.org/data/MOD10A2/versions/6>). This product of MODIS shows the snow cover (baseline: 8 days)  
157 and is also globally available at a resolution of 500 m. MOD10A2.006 snow cover data are available since 2000.

158 MODIS is used to extract the seasonal snow line elevations (average) during the past 20 years in the Amu Panj  
159 basin.

160

#### 161 *2.4 Terra MODIS MOD11C3.006 for land surface temperature analysis*

162 The evolution of land surface temperature was completed using MOD11C3.006 monthly products, 0.05 degrees  
163 (<https://lpdaac.usgs.gov/products/mod11c3v006/>). Temperature trends were analysed from 2000 through 2021  
164 (significance > 0.05 p-value) and the slopes were extracted and plotted on monthly maps.

165

#### 166 *2.6 Concept of the SAFE algorithm*

167 As the aim of this study is to detect and map the annual occurrence of **depositional** zones during the past 32 years  
168 within the study area, the monitoring approach must be reasonable and transferable from year to year. Based on  
169 frequent field observations and literature (Eckerstorfer et al., 2016), the authors noticed that **depositional** zones  
170 can be detected using the contrast between snow cover and bare cover, but the timing is perhaps the most important  
171 consideration. Indeed, the script is based on the assumption that snow packages exist in lowlands, especially along  
172 rivers and streams, as late as May through mid-July. At this time of the year, the terrestrial snow cover has largely  
173 melted and only snow packages triggered by avalanches remain. The location of those snow packages is also very  
174 critical (i.e., along riverbanks). These zones are indeed detectable by delineating the **depositional zones of the**  
175 **avalanches** (not their release or transition zones); in most cases these were located on river or stream banks as  
176 observed in the field because the hillslopes always route snow avalanches in this direction. We cannot differentiate  
177 between dry, wet, or powder snow because the process detects the remaining snow packages as avalanches in the  
178 late season (spring and summer), not in winter, nor can we delineate multiple **deposits** within the same depositional  
179 feature, only the combined **deposit zones**. In winter, we were not able to differentiate contrasts between snow cover  
180 and avalanches, thus our focus was on the late season.

181

#### 182 *2.7 Google Engine interface and code availability*

183 The concept of detecting the ‘remaining snow avalanches deposits in the late season’ was written in Java Script  
184 using the *Google Engine* platform. The script SAFE is available at:  
185 <https://code.earthengine.google.com/?scriptPath=users%2Farnaudcaiserman%2Fexport%3ASAFE>. We selected  
186 *Google Engine* for its relative simplicity of use and open access code, which is available to all stakeholders  
187 involved in hazard and vulnerability assessments. Additionally, internet connections in remote areas, such as  
188 within the Amu Panj basin, are limited and powerful computers required to run scripts and process big data are  
189 sparse. Our script can be run by anyone in a reasonable amount of time, even with a low internet capacity. As an  
190 example, yearly **depositional zones of avalanches** in our study area were downloaded and mapped from

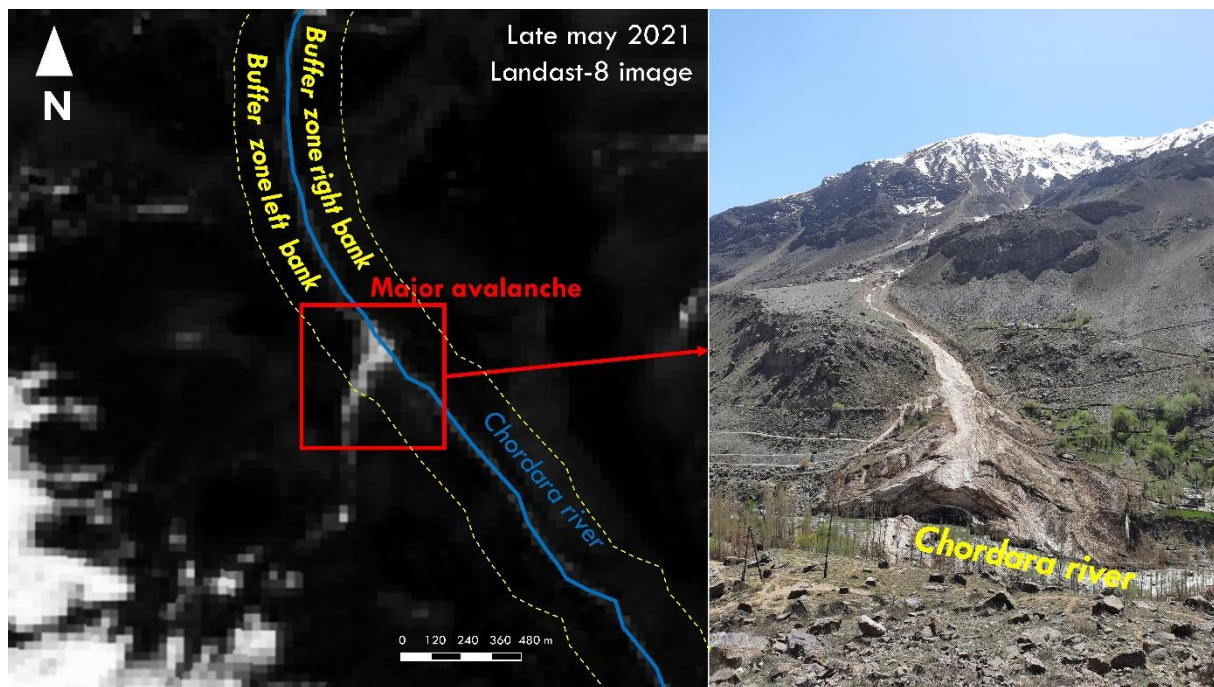
191 Badakhshan (SAFE was processed from Khorog, University of Central Asia campus, in Tajikistan) in 11.3 h (about  
192 20 min per year of record) with an average connection of 2.2 Gb/s.

193

### 194 2.8 Region of interest

195 The first step of SAFE is to define a region of interest as a mask to clip the Landsat images using SRTM-30 and  
196 MOD10A2.006. Avalanche deposits that terminated on riverbanks, rivers, and streams are derived from SRTM-  
197 30 DEMs using *ArcHydroTool* in *ArcGIS Pro Software*. Buffers of 200 m on both sides of rivers and streams are  
198 defined to: (1) catch the depositional zone of avalanches that terminate in rivers and (2) increase the probability of  
199 excluding the snow coverage in higher elevations that may remain throughout the summer. As an illustration, a  
200 major avalanche occurred in the border zone of Afghanistan and Tajikistan in winter 2021. The remaining  
201 depositional zone was still distinct in late May and June of that year on the bank of Chordara River (Figure 2).

202



203

204 **Figure 2. An illustration of avalanche **depositional zone** detection using late snow season Landsat-8 image**  
205 **near Khorog in May 2021 (Badakhshan in Tajikistan)**

### 206 2.9 Date range of interest

207 A 200 m riparian buffer was used as a mask to clip the Landsat images. Because our area of coverage encompasses  
208 very different elevations, the date of snow melt is not uniform throughout the basin. Therefore, distinguishing  
209 between the depositional zone and bare land requires different times depending on elevation. To accomplish this,

210 we calculated the average elevation of the snowline for the last 20 years using MODIS products. To distinguish  
 211 the different melt timing between highlands from lower areas, we selected the summer snowline (June-July-  
 212 August; JJA). The average elevation of the JJA snowline was 4420 m during the past 20 years. Two masks were  
 213 therefore produced: one with a river buffer in lowlands and another for highlands. Those masks are only relevant  
 214 if the user carefully selects the date of interest. For lowlands (below 4420 m), our time window was 15 May to 15  
 215 June, indicating that the script downloads and compiles all available Landsat images acquired in this range and  
 216 detects the **deposit zones** efficiently because during that period the terrestrial snow cover has already melted and  
 217 the deposits are easily recognised. For higher elevations (above 4420 m), snow cover melted later; dates to  
 218 accurately distinguish the remaining snow packages ranged from 15 June to 15 July. After many tests, it was  
 219 confirmed that these date ranges reproduced the desired snow conditions during the entire 32-y period. In the  
 220 script, users can modify these dates (line 24 and 112) to conform to local conditions.

221

### 222 *2.10 Snow index reclassification*

223 After the construction of the mask, SAFE proceeds as outlined in Figure 3. NDSI is selected to detect snow of  
 224 **deposit zones** in the script for its transferability from one Landsat generation to another. NDSI computes a ratio  
 225 between VIS and SWIR bands of Landsat satellites with negative NDSI representing non-snow cover and positive  
 226 values indicating snow coverage (Equation 1). Three cover types were distinguished to detect **depositional zones**  
 227 **of avalanches** at the correct time: (1) bare lands; (2) water bodies; and (3) snow. The values in Table 1 were  
 228 established after multiple tests before obtaining sufficient precision to distinguish **deposit zones** from other land  
 229 covers. On each mosaic (composite of the available images during the period of interest), a cloud mask is applied  
 230 using Landsat QA bands in the script to remove clouds from the scene.

231

$$\frac{\text{Band 4} - \text{Band 6}}{\text{Band 4} + \text{Band 6}} \quad \text{Equation 1}$$

232

233

**Table 1. NDSI discrete values for avalanche **depositional zones** detection**

<b>Coverage</b>	<b>NDSI values</b>
Bare soil	-1 to -0.05
Water bodies	-0.051 to 0.30
Snow cover	0.31 to 1

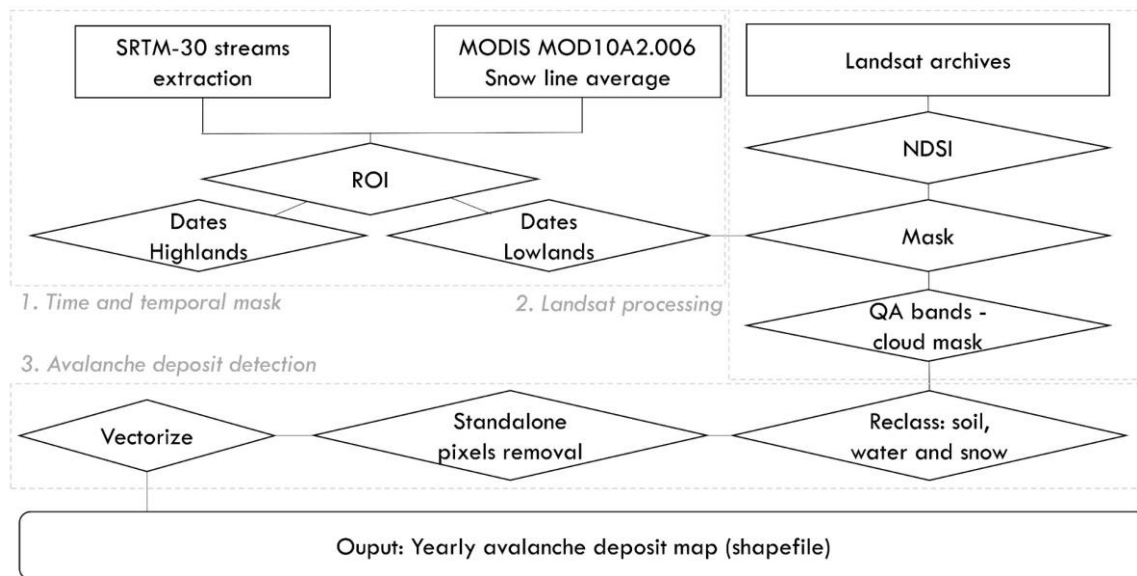
234

### 235 *2.11 Depositional zone selection*

236 This further step reclassifies annual NDSI layers using ranges of values in Table 1. Only ‘snow cover’ that  
 237 designates snow avalanche **deposit zones** is selected in the script. From the selected reclassification, the script  
 238 removes the standalone pixels because their classification might not be precise or representative of actual cover.



239 Next, the selected ‘avalanche pixels’ are verified into the script avoiding manual vectorization after the  
 240 downloading process. The vectorization procedure of **depositional zones of avalanches** is justified by the analysis  
 241 steps and post-processing after downloading data. **Depositional zones of avalanche** statistics, elevations, and  
 242 **surface areas** are extracted from vector files. Finally, annual **avalanche deposit zone** shapefiles are exported into  
 243 the Google Drive user’s account.



244  
 245 **Figure 3. Flow chart for Snow Avalanche Frequency Estimation (SAFE) using Landsat archives in Google**  
 246 **Engine.**

247  
 248 *2.12 Depositional zones of avalanche surface area classification*

249 Once the data are downloaded and imported into the GIS environment, statistical analysis commences. Every year,  
 250 the number and areas of **deposit zones** are calculated to quantify their evolution. Moreover, the **surface areas** of  
 251 the **depositional zones** are classified. Although a generic **surface area** classification exists (Greene et al., 2016),  
 252 we decided to classify avalanches by **surface areas** based on local conditions. We segregated four discrete  
 253 categories of **deposit zones**: small (< 1000 m<sup>2</sup>); medium (1000-5000 m<sup>2</sup>), large (5000-15,000 m<sup>2</sup>), and very large  
 254 (15,000-100,000 m<sup>2</sup>). Such a classification enabled us to assess the intensity and potential impact of those hazards  
 255 in specific locations. SAFE is not able to detect the avalanches at their time occurrence, and since these hazards  
 256 are detected weeks after initiation, their **surface area** is underestimated by SAFE due to melting. However, the  
 257 estimated **surface areas** in SAFE are still useful for classifying **depositional zones of avalanches** by **surface area**  
 258 since large snow deposits melt slower than small snow deposits. The small avalanches that occurred in winter will

259 appear as small deposit at the time of extraction in SAFE and the large events as large hazards since visible snow  
260 deposits can be seen in late spring.

261

### 262 **3. Results**

#### 263 *3.1 Validation*

264 The performance of SAFE in correctly detecting snow avalanche depositional zones required careful assessment.  
265 To achieve this, we collected datasets that show actual locations (Global Positioning System) of avalanches that  
266 occurred in the Amu Panj basin during the last 32 years. A total of 158 snow avalanche depositional zones were  
267 easily identified in the riparian buffer zones on Google Earth images in 2001, 2003, 2015, 2017, and 2019. No  
268 other Google Earth images were available during the last 32 years in Afghanistan, therefore the comparison  
269 between SAFE and the true events was conducted with those available 158 deposit zones. These 158 deposits were  
270 extracted from Google Earth and stacked with SAFE outputs. SAFE deposits were considered as valid when the  
271 two datasets were overlapped at the same location. Here we used statistical measures to assess the performance of  
272 SAFE through the Probability of Detection (POD; Equation 2, based on (Hafner et al., 2021)):

273

$$274 \quad \text{POD} = \text{true positive deposit zones} / (\text{true positive deposit zones} + \text{false negative deposit zones})$$

275 **Equation 2**

276

277 where *true positive deposit zones* are the avalanches detected by SAFE that were actually visible on Google Earth  
278 images (in valleys where GE images were available) and *false negative deposit zones* are the locations where SAFE  
279 did not detect *deposit zones* that had actually happened. Moreover, Positive Predictive Value (PPV; Equation 3)  
280 was calculated to assess the number of times SAFE found an actual *avalanche deposit zone* on the ground as  
281 follows:

282

$$283 \quad \text{PPV} = \text{true positive deposit zones} / (\text{true positive deposit zones} + \text{false positive deposit zones})$$

284 **Equation 3**

285

286 where *false positive deposit zones* are avalanche *deposits predicted* by SAFE that had never occurred.

287

288 The results suggest a good reliability of SAFE (Table 2). The overall POD is 0.77 which means that SAFE  
289 identified a significant number of the *depositional zones of avalanches* that impacted valley bottoms. Moreover, it  
290 seems that SAFE performs better in detecting true positive *deposit zones* (that occurred on the ground), as shown  
291 by the high PPV scores (average: 0.96). SAFE almost never detected *depositional zones of* avalanches that did not

292 exist. However, SAFE might miss some **deposit zones** due to cloud cover on the Landsat images, especially in  
 293 2001 (Table 2; POD = 0.42 in 2001).

294

295

**Table 2. Probability of detection and Positive Predictive Values of SAFE**

<b>Statistics</b>	<b>2001</b>	<b>2003</b>	<b>2015</b>	<b>2017</b>	<b>2019</b>	<b>Average</b>
<b>True positive</b>	10	35	12	19	48	
<b>False negative</b>	14	6	1	4	9	
<b>False positive</b>	1	0	0	1	3	
<b>POD</b>	0.42	0.85	0.92	0.83	0.84	<b>0.77</b>
<b>PPV</b>	0.91	1.00	1.00	0.95	0.94	<b>0.96</b>

296

297 Another source of error arises when SAFE cannot detect **depositional zones** due to a dark color on the snow surface  
 298 associated with surface debris or a debris flow on top of the **deposit zones**. NDSI may have identified those debris  
 299 layers as bare soil in the classification. Based on our findings, SAFE can be considered as a conservative, yet  
 300 robust and efficient tool to automatically identify snow avalanche depositional zones in very remote areas and can  
 301 be applied in any mountainous region.

302

### 303 *3.2 SAFE outputs compared with outlined avalanches using SPOT-6 images*

304 As a potential method of strengthening our testing of SAFE, outputs of our model were compared with a method  
 305 that applied a more precise and expensive remote sensing product in Switzerland in 2018 (Bühler et al., 2019).  
 306 The Swiss area encompassed 12,500 km<sup>2</sup> where more than 18,000 snow avalanches were manually digitized using  
 307 very high-resolution products SPOT-6 images (in January 2018). While our dataset is quite different from the  
 308 Swiss data, the objective of this comparison was to assess how many snow avalanche deposits SAFE could detect  
 309 compared to the approach using SPOT-6 (Table 3).

310

311 **Table 3. Comparison of snow avalanches deposits zones between SAFE outputs (April to June 2018) and**  
 312 **manual digitization using high-resolution SPOT-6 images in Switzerland in January 2018\***

<b>Method</b>	<b>Number of snow polygons</b>	<b>Area of snow polygons (m<sup>2</sup>)</b>
SPOT digitization	7574	362,187,741
SAFE detection	9948	494,454,599
Overlapping SPOT-SAFE	2194	223,907,868

313 \*SPOT data based on (Bühler et al., 2019)

314

315 Importantly, not all avalanches manually digitized on SPOT-6 images were comparable to SAFE results. To make  
316 this comparison more consistent, we clipped the outlined avalanches with the valley bottom mask used in SAFE.  
317 Following this modification, the SPOT-6 digitization process identified 7574 avalanche deposits in valley bottoms  
318 compared with 9948 by SAFE. Overlapping these two datasets, we found that both approaches detected 2194  
319 deposit zones in common. Much of this discrepancy is due to the timing of SAFE images, which examine deposits  
320 that remain in late spring and early summer, whereas SPOT digitization covered only January. The larger number  
321 of snow deposits detected by SAFE occur during late season snow avalanches that impact valleys. This suggests  
322 that SAFE could not detect all January snow deposits because many of those already melted by the time of SAFE  
323 detection (early April to late June in the Swiss case). In addition, optical image quality strongly depends on cloud  
324 cover that may cause avalanches to be obstructed. For instance, we could not compare the 2019 SPOT-6 derived  
325 dataset in eastern Switzerland (Hafner et al., 2021) due to cloudy images at the end of winter and early spring  
326 because these snow avalanches had already melted, implying that SAFE is more suitable for high mountain areas  
327 (>4000 m) where snow deposits remain longer in valleys, thus inflicting greater damages and obstructions. Using  
328 LANDSAT images, SAFE somewhat circumvents this problem of cloud cover by assessing many years of data  
329 (in our case 32 y). However, SAFE does not distinguish individual events and considers overlapping snow deposits  
330 as one, in contrast to SPOT-6 which distinguishes these as discrete events. This, in addition to the different methods  
331 and spatial resolution difference between SAFE and SPOT, explains the somewhat low number of overlapping  
332 snow deposits between SAFE and SPOT. Moreover, the SPOT digitization procedure found a total avalanche area  
333 of 362,187,741 m<sup>2</sup> in January, while SAFE detected 494,454,599 m<sup>2</sup> of deposits at the end of the avalanche season,  
334 including 223,907,868 m<sup>2</sup> in common. The area detected by SAFE is naturally larger than SPOT-6 since SAFE  
335 maps all detectable deposits at the end of the winter. Moreover, SAFE did not detect the small avalanches of  
336 January that rapidly melted after they occurred. The polygons extracted by SAFE using Landsat images are  
337 obviously coarser than those outlined with SPOT-6 images, which partly explains the low number of overlapping  
338 snow deposit zones, but a much more comparable detected area (62%) between the two methods. Much of the  
339 discrepancy is related to SAFE's inability to detect individual events and missing deposits that rapidly melt (mostly  
340 from the early winter snow avalanches), as well as the very different resolution of these products.

341

### 342 3.3 Snow avalanche *depositional zone* frequency from 1990 to 2021

343 By compiling 32 years of satellite images (see Methodology), the frequency of avalanche *depositional zones* at a  
344 900 m<sup>2</sup> pixel scale was determined (Figure 4 and 5a). SAFE inventories snow avalanche *deposits* that occurred  
345 within a year and therefore identifies the most vulnerable areas, but it does not aim to forecast future avalanches.  
346 During this period, some 810,000 *depositional zones* impacted valleys within the Amu Panj basin (28,500 km<sup>2</sup>),  
347 i.e., approximately 28 *depositional zones* km<sup>-2</sup>. Each year these avalanche deposits cover an average of 1.23% of

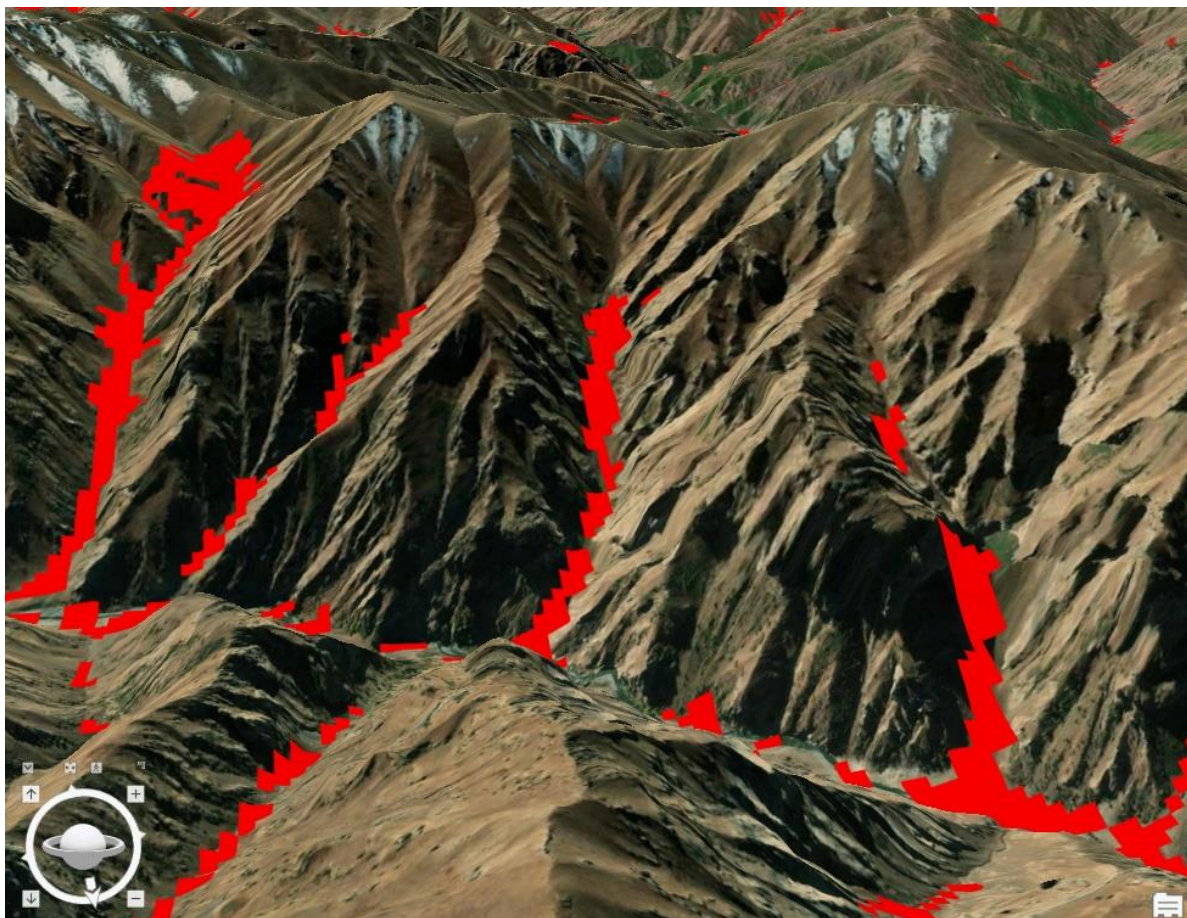
348 the basin area but **surface area** varies from year to year. Avalanche **depositional zone surface area** ranged from 900  
349 to 100,000 m<sup>2</sup> and is categorized into four classes: small (< 1000 m<sup>2</sup>); medium (1000-5000 m<sup>2</sup>), large (5000-15,000  
350 m<sup>2</sup>), and very large (15,000-100,000 m<sup>2</sup>). The most frequent are medium **surface area deposit zones**; 342,000  
351 events during the past 32 years. Our approach also identifies very large snow avalanches **depositional zones** that  
352 pose the greatest danger to local populations and infrastructure. We found no correlation between altitude of  
353 depositional zones and their **surface areas**. Avalanches deposits in this region have an average altitude of 3820 m  
354 and the lowest **depositional zone** occurred at 1755 m.

355

356 These spatial and temporal statistics allow for a geographic assessment of the avalanche **deposits**. In total, ten sub-  
357 catchments (ranging from 18 to 240 km<sup>2</sup>) were impacted by more than one avalanche **depositional zone** km<sup>-2</sup>y<sup>-1</sup>,  
358 with an average frequency of 0.26 **deposit zones** km<sup>-2</sup>y<sup>-1</sup> throughout the Panj Amu basin (Figure 6). More  
359 importantly, these maps prioritize villages prone to avalanches **deposits** and inform relevant stakeholders which  
360 villages and infrastructure are most at risk. Of the 4154 villages in the region, 50 are impacted by at least one  
361 avalanche within a 1 km radius each year (Figure 7). These susceptible villages are in Upper Badakhshan in the  
362 north of our study area and in the Wakhan Corridor in the east where the highest mountains and most remote  
363 villages are located. During the 32-y period, 92 villages were affected by very large avalanches **depositional zones**  
364 in Badakhshan and Wakhan. Since 2019, Aga Khan Agency for Habitat (AKAH) is monitoring villages of  
365 Afghanistan that have been impacted by snow avalanches. In total, 217 villages have been impacted by avalanches  
366 **deposit zones** and those are located in the same vulnerable valleys detected by SAFE, namely High Badakhshan  
367 and the Wakhan corridor.

368

369 Our remote sensing approach facilitates innovation in snow avalanche **depositional zone** monitoring: i.e., detecting  
370 avalanches **deposits** outside of populated areas, especially along roads that are frequently blocked by avalanches  
371 (Figure 8). More than 2000 roads in the basin (5.47% of the road network) were affected by avalanches **deposits**  
372 every year. Additionally, more than 400 roads in Upper Badakhshan and Wakhan regions experienced more than  
373 2 avalanches **depositional zones** y<sup>-1</sup> km<sup>-1</sup> of road (within a 1 km buffer). The average frequency along roads is 0.86  
374 avalanche **deposits** km<sup>-1</sup>y<sup>-1</sup> during the past 32 years, most of these in the medium- **surface areas** category.



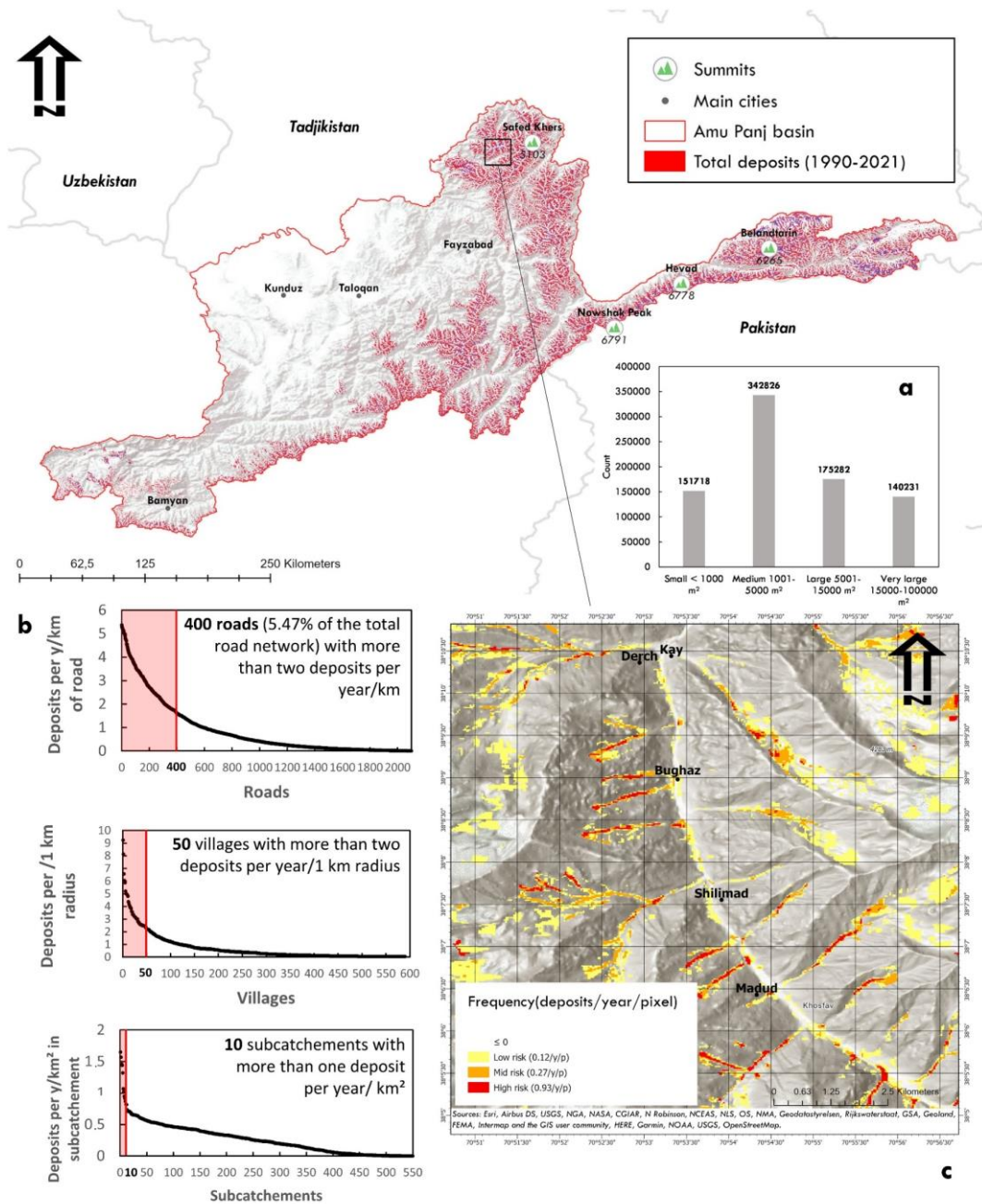
375

376

377

378

**Figure 4. 3-Dimension view of the 32 years avalanche **depositional zones** maps in Khinj village in Afghanistan (*ArcGisPro*)**



379

380 **Figure 5. Yearly inventory map of snow avalanche depositional zones in the Amu Panj basin: 1990-2021:**

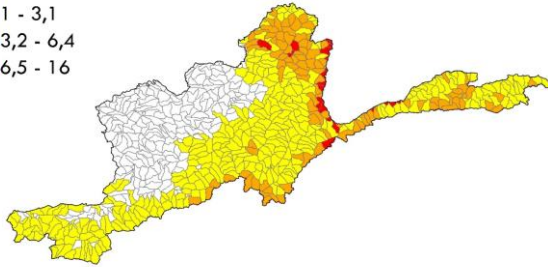
381 **a, Surface area classification of avalanche depositional zone frequency; b, Avalanche depositional zone**

382 **frequency per number of roads, villages, and subcatchments in the basin; c, An example map of avalanche**

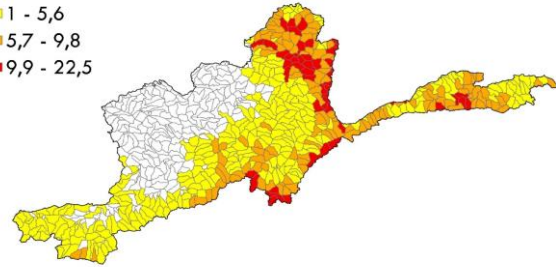
383 **depositional zone frequency during the 32-y period at a village scale.**

Total snow avalanches deposits per km<sup>2</sup> in subcatchments (category 1) Total snow avalanches deposits per km<sup>2</sup> in subcatchments (category 2)

□ 0  
■ 1 - 3,1  
■ 3,2 - 6,4  
■ 6,5 - 16



□ 0  
■ 1 - 5,6  
■ 5,7 - 9,8  
■ 9,9 - 22,5



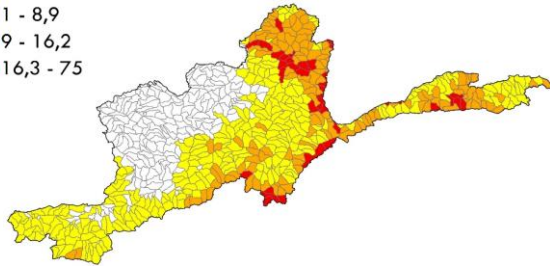
90 45 0 90 180 270 360  
Kilometers



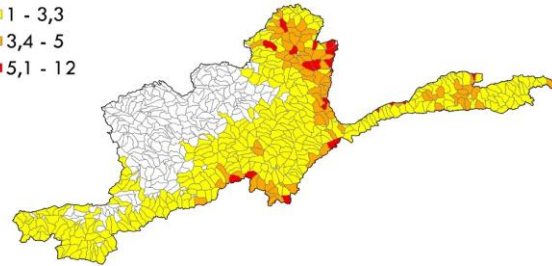
384

Total snow avalanches deposits per km<sup>2</sup> in subcatchments (category 3) Total snow avalanches deposits per km<sup>2</sup> in subcatchments (category 4)

□ 0  
■ 1 - 8,9  
■ 9 - 16,2  
■ 16,3 - 75



□ 0  
■ 1 - 3,3  
■ 3,4 - 5  
■ 5,1 - 12



385

386

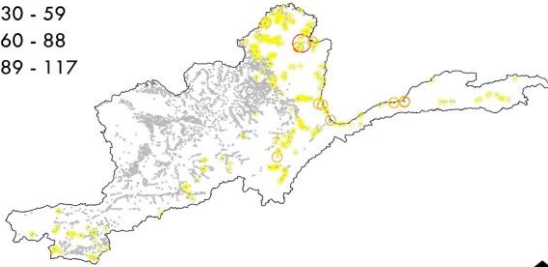
**Figure 6. Total avalanche **depositional zones** per category and per square kilometer in subcatchments during the past 32 years.**

387



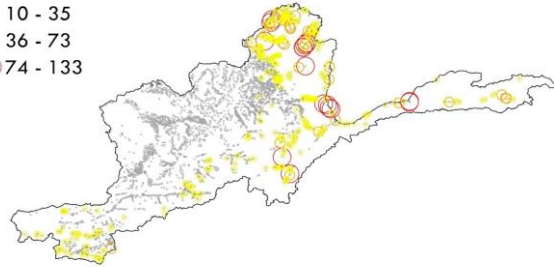
Total snow avalanches deposits per village (category 1)

- 0
- 30 - 59
- 60 - 88
- 89 - 117



Total snow avalanches deposits per village (category 2)

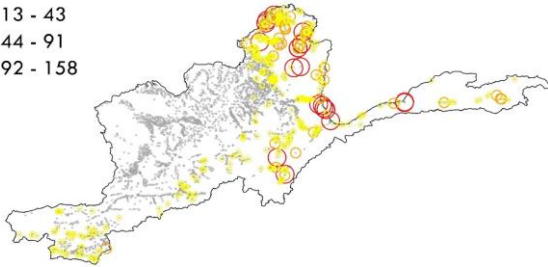
- 0
- 10 - 35
- 36 - 73
- 74 - 133



388

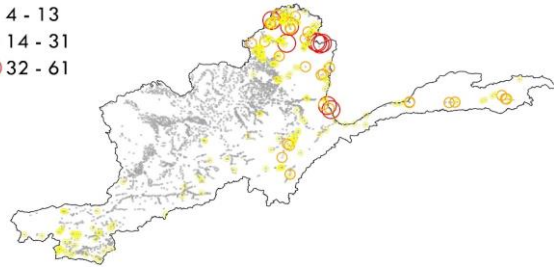
Total snow avalanches deposits per village (category 3)

- 0
- 13 - 43
- 44 - 91
- 92 - 158



Total snow avalanches deposits per village (category 4)

- 0
- 4 - 13
- 14 - 31
- 32 - 61

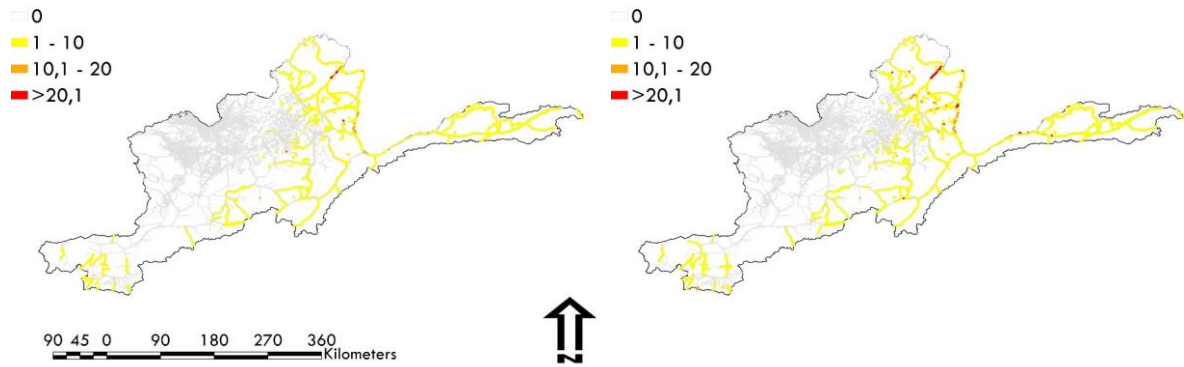


389

390

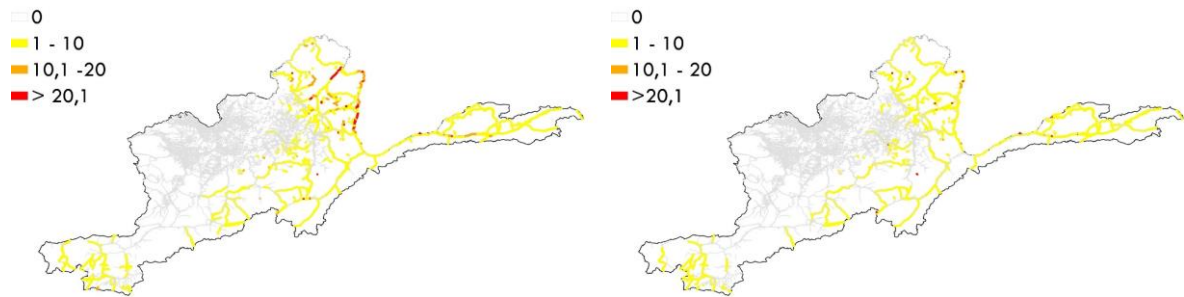
Figure 7. Total avalanche **depositional zones** per category and per village during the past 32 years.

Total number of avalanches deposits per kilometer of road (category 1) Total number of avalanches deposits per kilometer of road (category 2)



391

Total number of avalanches deposits per kilometer of road (category 3) Total number of avalanches deposits per kilometer of road (category 4)



392

393

**Figure 8. Total avalanche **depositional zones** per category and per kilometer of roads during the past 32 years**

394

395

396

397

398

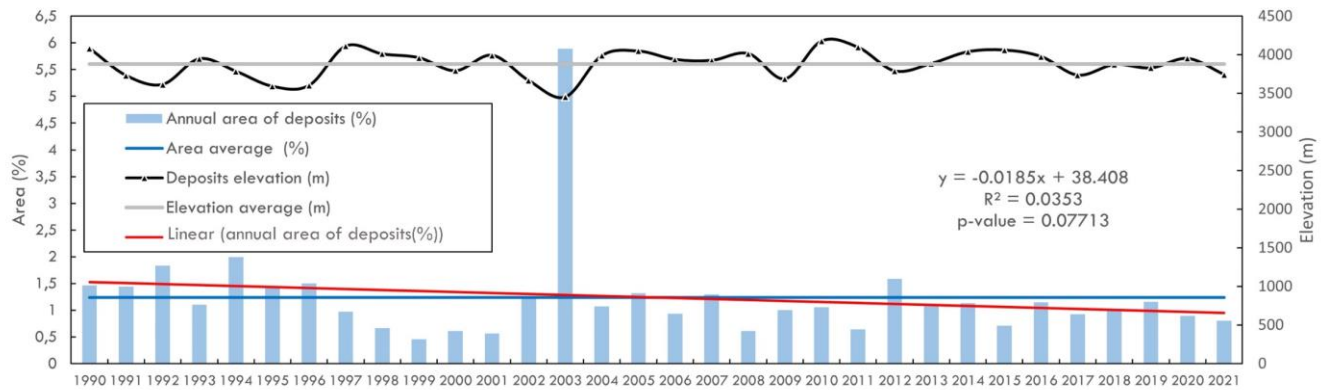
400 *3.4 Stream blocking and resultant flooding*

Damages to infrastructure and blocking of roads by avalanche deposits are not the only consequences of these mountain hazards. Because depositional zones typically reach rivers in this steep, incised terrain, the sudden and rapid arrival of several tons of snow can temporarily block rivers inducing short-term localized flooding. By cross-checking the map of the rivers in the Amu Panj basin with SAFE outputs, it appears that 26.2% of the river network is impacted by avalanche deposits, mainly  
405 in the high mountains. During the past 32 y, 12% of the streams have been blocked by at least 10 avalanche **deposits** km<sup>-1</sup> representing a significant risk for villages and farms in floodplains. The accumulated snow mass impounds river water until it can break through releasing a large discharge surge. Thus, depending on the **surface area** of the avalanche **deposit** with respect to the channel dimensions, damages to villages and farmlands may occur both upstream due to impounded water (hours to weeks) and to downstream following the sudden release of water.

410

*3.5 Snow **avalanche depositional zone** trends during the past 32 years*

This long-term monitoring of snow avalanche **deposits** facilitates the assessment of the evolution of these rapid mass movements. During the 32 years of avalanche **depositional zone** assessment, no significant temporal trends in impacted areas were detected (Figure 9). In addition, there was no significant trend of the surface are of snow **deposits** (p-value > 0.05).  
415 Nevertheless, some years posed much greater risk than others. In the last 32 years, ten years have been more at risk with above-average avalanche **deposit** coverage: 1990, 1991, 1992, 1993, 1994, 1995, 1996, 2003, 2005, 2007 and 2012. In particular, 2003 had many avalanche **depositional zones** that occupied almost 6% of the surface area of the entire basin. That year was locally noted as having heavy snowfall and farmers benefited from more snowmelt in the spring, leading to higher than average crop yields in 2003 (FAO, 2003; Guimbert, 2004). Notably, the higher risk years were also characterised by lower altitudes for  
420 avalanche **deposits**. There is a slight negative correlation (-0.55, Pearson test) between altitude and total annual avalanche area. With larger avalanche areas, deposits reach closer to villages. For example, in 2003, the lowest avalanche **depositional zone** occurred at an altitude of only 1871 m, very close to housing clusters and roads. It is therefore possible that communities below 2000 m are also impacted by snow avalanche **deposits** and in many mountain regions of the world this represents a significant proportion of the communities living proximate to these altitudes.



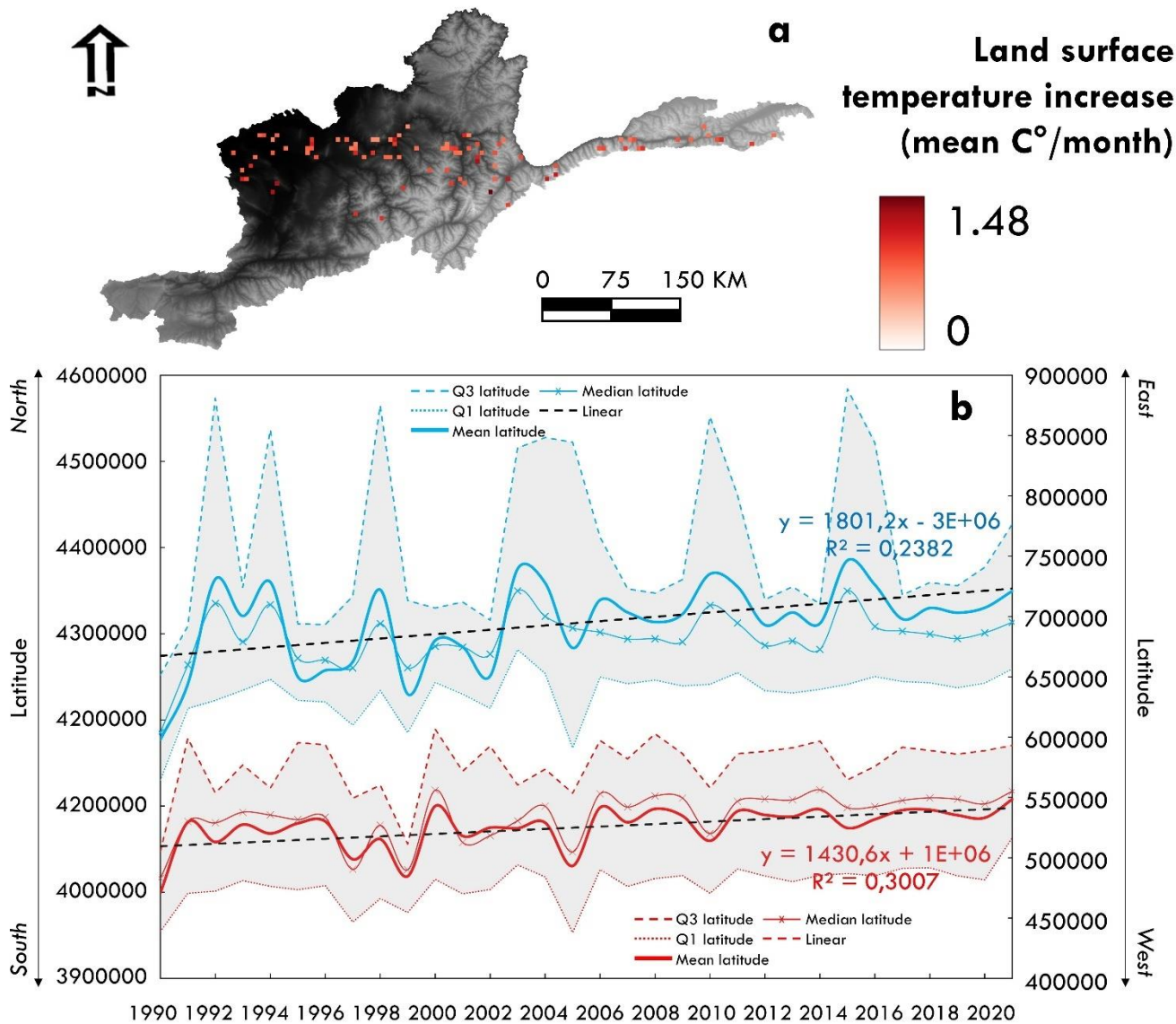
425

**Figure 9. Snow avalanche *depositional zone* area and elevation trends since 1990 in the Amu Panj basin. Elevation was calculated within each polygon of avalanche *deposits* using SRTM-30 Digital Elevation Model. Mann-Kendall p-value 0.05 test was conducted to assess the significance of the trend.**

430 *3.6 Temporal geographic shifts of snow avalanches *deposit zones**

Long-term monitoring also shows the evolution of the spatial distribution of snow avalanche *depositional zones*. The pattern of snow avalanche *deposits* has changed with time and slightly shifted to the northeast portion of the basin; thus, more avalanches are now occurring in the northeast than in the southwest (Figure 10a and b). Nevertheless, snow coverage did not shift simultaneously according to our remote sensing analysis nor did the snowline evolve, but rather remained variable over the last 32 years. The geographic shift of avalanche *depositional zones* is therefore likely due snow depth evolution. Deeper snowpacks trigger snow avalanches. There are no available data on snow depth at such a scale. *However, the slope was calculated and a Mann-Kendal test was applied for each pixel of the land surface temperature images (MOD11C3).* Remotely sensed land surface temperature changed during the last 20 years (Figure 10 a), with a warmer band occurring through the central portion of the basin in December (p-value 0.03 with an increase of 0.88 C°y<sup>-1</sup>). This central portion is mainly mountainous and this temperature pattern may have shifted the avalanches to the northern mountains of the area, while the south is characterized by lower mountains. Overall, avalanche *depositional zone* locations tend to follow the spatial distribution of snow depth (Bühler et al., 2016). This means that despite the high variability of the snow line and snow coverage, the distribution of snow avalanche *deposits* can significantly change over time in response to temperature changes and local communities must be prepared for shifting hazards.

440



445

**Figure 10. a, Map of areas with significant increases in monthly land surface temperatures in the Amu Panj Basin based on MOD11C3 products from 2000 to 2021; b, Geographical shift of avalanche deposits: mean longitude and latitude of avalanche deposits each year since 1990 show evidence of a movement to the northeast due to increasing winter temperature in mountainous areas.**

450

#### 4. Uncertainties and implications

##### 4.1 Sensitivity analysis of SAFE

To better understand how SAFE works and assess its performance, a sensitivity analysis was conducted between the model parameters. The number and surface areas of avalanche depositional zones vary according to the buffer used, the dates of

455 Landsat images, and finally the NDSI range during the snow classification. The sensitivity analysis was conducted for the year 2019 when SAFE was most robust in valleys where actual avalanche deposits were quite visible on Google Earth images (POD: 0.84 and PPV: 0.94). First, we run SAFE with different buffer widths (25 m of difference between each buffer). There is a strong positive correlation (0.98) between the number of avalanche deposits detected by SAFE and the buffer width (Figure 11a). The wider the buffer around the rivers, the more avalanche deposits SAFE will detect. On the other hand, for narrower buffers, the average surface area of avalanche depositional zones is smaller (positive correlation of 0.71). This is because a large buffer extends upslope where small snow patches reside, which are not avalanche deposits since they are located at the top of hillslopes. This means that the user should not select a buffer that is too wide, rather the area should only include the riparian zone of rivers and streams where the snow avalanche deposits are located. As such, we used a value of 200 m for the entire region studied.

465

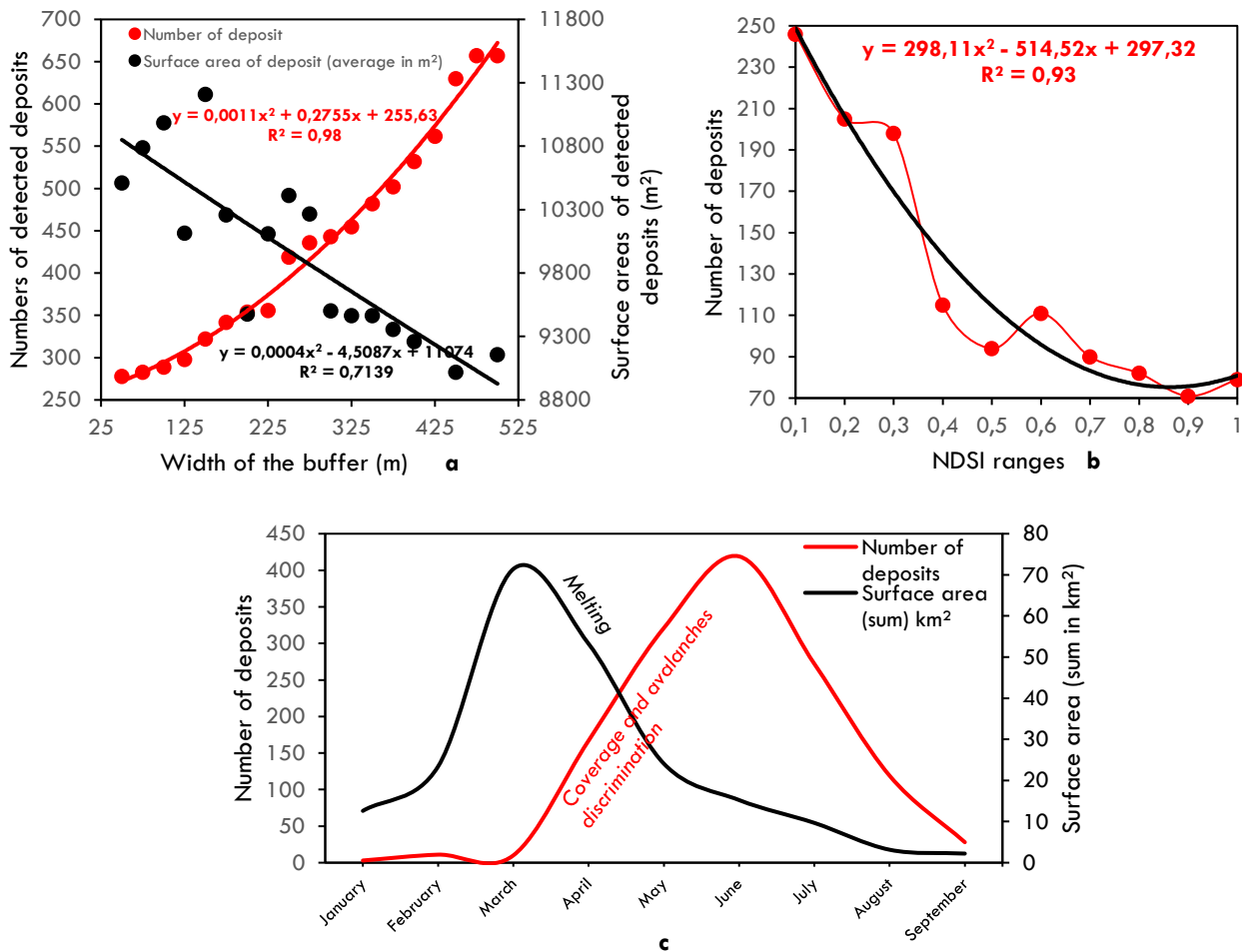


Figure 11. Sensitivity tests of SAFE for number and surface areas of detected avalanche depositional zones: a, width of buffer; b, NDSI ranges; and c, dates of interest

The number and **surface areas** of avalanche **depositional zones** detected by SAFE depends on the NDSI range when classifying snow. NDSI is used to differentiate between water bodies, bare lands, and snow. By varying the NDSI ranges of snow in the script, we notice a strong positive correlation with the number of avalanches **deposits** detected by SAFE. The closer the index is to 0, the more hazards SAFE finds. However, this correlation shows us that the choice of NDSI range is important because we notice a threshold at 0.31 (Figure 11b). Avalanche **depositional zones** seem to be more numerous with an NDSI lower than 0.31 because the snow pixels are confused with water bodies. It is therefore essential for the user to select an NDSI higher than 0.31 to distinguish water bodies (rivers, flood areas or lakes) and snow. However, there is no correlation between the NDSI ranges and the average surface areas of avalanche **deposits** because NDSI cannot interpret pixels other than 'snow' above the 0.31 threshold. Finally, the date of interest is a key parameter in SAFE. The number of avalanche **depositional zones** detected by SAFE is highest at the end of winter due to the almost constant cloud cover since January, but also due to the inability to distinguish avalanche **deposits** from snow cover in winter (with Landsat images) (Figure 11c). May is a key month for SAFE applications in high mountains: the snow coverage, which is thinner than the avalanche **depositional zones**, begins to melt and the number of avalanche **deposits** detected can then be assessed. It is therefore essential to select post-May images to detect avalanche **deposits** while taking care not to select post-July images as avalanches **deposits** melt in summer precluding detection.

485

Some avalanche deposits are also visible on successive images after the snow cover melts. SAFE was specifically designed to detect avalanche **depositional zones** at their earliest stage after snow melts. Indeed, starting from May (when the avalanche **deposits** are not confused with snow coverage), snow avalanche deposits start to melt and the **surface area will begin to** be underestimated. For that reason, it is important to select late spring images for lowland avalanche **depositional zones** and early summer for high land **deposits**, not later. Cloud cover is another issue in avalanche **deposit** locations and **surface area** detection since cloud cover may partly or fully obstruct the avalanche **deposits** at the time of the image. This is another reason to select images starting from late spring when regional cloud cover is lowest and even absent in early summer. If cloud cover is high even late spring, the users can still select later images, but there will be a risk that detected avalanche deposits will have started to melt. To summarize, we recommend the following three parameters in the SAFE script: buffer of 200 m to include only snow avalanche deposits;  $NDSI > 0.31$  to distinguish water bodies from snow, and images from May to July to distinguish avalanches **depositional zones** from snow cover.

#### 4.2 Excluding snow coverage

Interpreting the remaining snow packages as avalanche deposits can lead to some errors. Indeed, despite a precise masking operation (excluding summits and very high plateaus where snow persists), in some cases the use of NDSI might not properly segregate avalanche **depositional zones** from large areas of remaining snow. After assessing the **surface area** of true avalanche **deposits** (the ones that SAFE correctly detected based on Google Earth images), it appeared that snow cover  $> 100,000 \text{ m}^2$  were not avalanche **depositional zones** but rather snow cover; thus, these were removed. However, in highlands, even along

riverbanks, some snow packages interpreted as avalanche **depositional zones** may be remaining snow cover. As such, the date  
505 range for highlands was selected as late as possible in the year. Thus, it is advised to keep the mask at the very bottom of  
valleys (maximum 200 m buffer along the river) to exclude high plateaus and potential snow-covered areas.

#### *4.3 Water bodies in SAFE*

A final limitation of using this remote sensing and NDSI approach for avalanche **deposit** detection is the possible confusion  
510 between some small water bodies and avalanche **depositional zones**. Indeed, in some cases certain river reaches (stream order  
> 4 in our study area) could be interpreted as snow because they were frozen and appeared as white pixels on Landsat archives.  
The same issue can occur with ponds and lakes. This limitation was foreseen before processing the images in our study and  
we excluded these large water bodies from the region of interest (in the mask) by using available shapefiles. For example,  
Shiva Lake, one of the largest water bodies in Amu Panj basin (15 km<sup>2</sup>), was removed from the analysis. Another way to avoid  
515 the water pixel selection is to adapt the NDSI reclassification itself, depending on the study area. This is possible in the script  
lines 51-53 for low elevations and lines 139-141 for high elevations in the script.

#### *4.4 SAFE outcomes compared to other snow avalanches detection studies*

SAFE contributes to the literature on snow avalanche detection, but in a unique way using remote sensing. As noted, many  
520 studies and models exist using various products: Radar, Optical, and Topographic. The strength of remote sensing is the  
automatic processing at a large scale and over long timeframes. SAFE uses the capabilities of remote sensing by processing  
more than one image per year at the catchment scale. Moreover, the use of Landsat archives allows assessment over the last  
32 years, which is not yet possible with recent Radar data such as Sentinel-1. Most of the current avalanche detection models  
use freely available products, with acceptable if not good accuracy (Table 4). The accuracy of these studies using Radar images  
525 ranges from 53 to 81% making this a relatively robust tool. One of the reasons why SAFE does not use Radar images is the  
weight of the images (data storage), especially Sentinel-1, which is mostly above 1 Gb/image. These heavy images are not  
suitable for a model like SAFE, which was specifically designed for remote study areas where internet connections may be  
very limited. Other models also exist with Optical images with high accuracy ranging from 71 to 93% (Table 4). In the optical  
domain, SAFE showed a POD of 77% over an area of 28,500 km<sup>2</sup>. SAFE is therefore in the high range of models with optical,  
530 medium resolution (Landsat) images.

535



**Table 4. References on snow avalanche accuracy using remote sensing products (Radar, Optical and Terrain)**

Reference	Accuracy (%)	Dataset
Eckerstorfer et al., 2017	75	S1
Malnes et al., 2015	53*	S1
Martinez-Vazquez	76	GB-SAR LISA
Tompkin and Leinss, 2021	81	S1
Leinss et al., 2020	70	S1 and TerraSAR-X
Vickers et al., 2016	60	S1
Karas et al., 2021	70	S1
Yang et al., 2020	75**	S1
Singh et al., 2019	93	L8
Yarivan et al., 2020	90	Google Earth imagery
Hafner et al., 2021	74**	SPOT
Bühler et al., 2018	95**	DTM

\*55 avalanches were detected using S1 image out of 102 on the field.

540 \*\*POD

## 5. Conclusion

SAFE can be considered as a universal approach to assess snow avalanche **depositional zones** where ground data are very limited, such as in the Afghan mountains. Here we showed the capability of long-term remote sensing data to robustly detect snow avalanche **deposits** that impact valley locations. While we have successively applied SAFE to assess the frequency and impacts of avalanche **deposits** in valleys and lower hillslopes of Afghanistan, arguably one of the most data-limited regions worldwide, this model should perform even better in areas where snow data are available making it an important tool for avalanche vulnerability assessment worldwide. More than 30 years after the launch of Landsat-5, it is now possible to compile all data and assess the temporal as well as spatial evolution of such hazards. NDSI is a relevant index to detect avalanches when selecting the correct region and dates of interest - i.e., riverbanks during the late melt season. The thickness of the depositional zones facilitates the detection of these avalanche deposits after the snow cover has melted on hillslopes in spring or early summer. **Moreover, the application of SAFE in Afghanistan, compared to its application in Switzerland, showed that the script can be applied worldwide, especially in high mountains (above 4000 m) since deposit zones are still detectable in late spring at those elevations.**

555 The automation of snow avalanche detection using remote sensing technologies at regional scales is still new and SAFE was designed to guide decision-makers, planners, and disaster risk practitioners. Indeed, such people can now know where the most at-risk areas are located based on these frequency maps. Such information informs the relative risk of building sites and land use decisions in such mountainous terrain with greater precision. The level of exposure of roads to avalanche **depositional zones** can also be estimated using these frequency maps, and can inform road planners and managers regarding road location,

560 maintenance practices, and mitigation structures. Moreover, villages of high mountains such as in Afghanistan are strongly highly dependent on roads connections to provide necessary food, energy, medical supplies, and life-support items, especially in winter. It is therefore critical for local decision makers to assess the frequency of road blockage by avalanche deposits. Thus, open-access and user-friendly tools such as SAFE are highly applicable to interests of local stakeholders even with medium to low power computers since SAFE uses Google servers. The tourism sector can also benefit from this snow avalanche deposit  
565 inventory, especially the winter sports industry. Furthermore, this method can also be used to prioritize areas for more sophisticated and data-intensive avalanche risk analysis (Keylock et al., 1999). SAFE can be applied by any user throughout mountainous regions of the world as it is designed to be user-friendly, and frequent users can contribute to the robustness of the snow avalanche deposit archive, thus improving recommendations for policy makers.

#### 570 **Author contributions**

A.C. designed the concept of SAFE method, wrote the Google Engine script and processed the analyses of snow avalanches. A.C. and R.C.S. participated the conception of SAFE and all authors helped interpret the results. D.R.G. contributed to the writing and provided the AKAH dataset of impacted villages by snow avalanches. A.C. and R.C.S. wrote the paper.

#### 575 **Competing interests**

The authors declare that they have no conflict of interest.

#### **Acknowledgements**

The authors are very thankful to Nusrat Nahab, Head of Emergency Management Aga Khan Agency for the Aga Khan Agency  
580 for Habitat for her support in this study and for sharing information about snow avalanches in Afghanistan. This study was implemented under the ongoing project "Addressing Climate Change in Afghanistan (E3C)" funded by the European Union, in close collaboration with Aga Khan Foundation and Wildlife Conservation Society based in Afghanistan.

#### **References**

- 585 Abermann, J., Eckerstorfer, M., Malnes, E., Hansen, B.U., 2019. A large wet snow avalanche cycle in West Greenland quantified using remote sensing and in situ observations. *Nat Hazards* 97, 517–534. <https://doi.org/10.1007/s11069-019-03655-8>
- Asad Sarwar, Q., 2002. Water resources management in Afghanistan: the issues and options. International Water Management Institute, Pakistan.
- Bair, E.H., Rittger, K., Ahmad, J.A., Chabot, D., 2020. Comparison of modeled snow properties in Afghanistan, Pakistan, and Tajikistan. *The Cryosphere* 14, 331–347. <https://doi.org/10.5194/tc-14-331-2020>
- 590 Barbolini, M., Pagliardi, M., Ferro, F., Corradeghini, P., 2011. Avalanche hazard mapping over large undocumented areas. *Nat Hazards* 56, 451–464. <https://doi.org/10.1007/s11069-009-9434-8>
- Bühler, Y., Adams, M.S., Bösch, R., Stoffel, A., 2016. Mapping snow depth in alpine terrain with unmanned aerial systems (UAS): potential and limitations. *The Cryosphere* 10, 1075–1088. <https://doi.org/10.5194/tc-10-1075-2016>

- 595 Bühler, Y., Hafner, E.D., Zweifel, B., Zesiger, M., Heisig, H., 2019. Where are the avalanches? Rapid SPOT6 satellite data acquisition to map an extreme avalanche period over the Swiss Alps. *The Cryosphere* 13, 3225–3238. <https://doi.org/10.5194/tc-13-3225-2019>
- Bühler, Y., von Rickenbach, D., Christen, M., Margreth, S., Stoffel, L., Stoffel, A., Kühne, R., 2018a. Linking modelled potential release areas with avalanche dynamic simulations: an automated approach for efficient avalanche hazard indication mapping. *International snow science workshop proceedings 2018* 810–814.
- 600 Bühler, Y., von Rickenbach, D., Stoffel, A., Margreth, S., Stoffel, L., Christen, M., 2018b. Automated snow avalanche release area delineation – validation of existing algorithms and proposition of a new object-based approach for large-scale hazard indication mapping. *Natural Hazards and Earth System Sciences* 18, 3235–3251. <https://doi.org/10.5194/nhess-18-3235-2018>
- 605 Chabot, D., Kaba, A., 2016. Avalanche forecasting in the Central Asian countries of Afghanistan, Pakistan and Tajikistan. Presented at the International Snow Science Workshop, Breckenridge, Colorado.
- Colorado Avalanche Information Center, 2021. *Avalanche.org* » Accidents [WWW Document]. *Avalanche.org*. URL <https://avalanche.org/avalanche-accidents/> (accessed 6.30.21).
- Deems, J.S., Painter, T.H., Finnegan, D.C., 2013. Lidar measurement of snow depth: a review. *Journal of Glaciology* 59, 467–479. <https://doi.org/10.3189/2013JoG12J154>
- 610 Eckerstorfer, M., Bühler, Y., Frauenfelder, R., Malnes, E., 2016. Remote sensing of snow avalanches: Recent advances, potential, and limitations. *Cold Regions Science and Technology* 121, 126–140. <https://doi.org/10.1016/j.coldregions.2015.11.001>
- Eckerstorfer, M., Malnes, E., Frauenfelder, R., Doomas, U., Brattli, K., 2014. Avalanche Debris Detection Using Satellite-Borne Radar and Optical Remote Sensing. *International Snow Science Workshop 2014 Proceedings, Banff, Canada* 131–138.
- Eckerstorfer, M., Malnes, E., Müller, K., 2017. A complete snow avalanche activity record from a Norwegian forecasting region using Sentinel-1 satellite-radar data. *Cold Regions Science and Technology, International Snow Science Workshop 2016 Breckenridge* 144, 39–51. <https://doi.org/10.1016/j.coldregions.2017.08.004>
- 620 European Avalanches Warning Services, 2021. Fatalities [WWW Document]. EAWS. URL <https://www.avalanches.org/fatalities/> (accessed 6.30.21).
- FAO, 2003. FAO global information and early warning system on food and agriculture - world food programme [WWW Document]. URL <https://www.fao.org/3/j0156e/j0156e00.htm> (accessed 10.17.21).
- GFDRR, 2018. Afghanistan Multi-Hazard Risk Assessment. World Bank, Kabul, Afghanistan.
- 625 Greene, E., Birkeland, K., Elder, K., McCammon, I., Staples, M., Sharaf, D., 2016. *Observation Guidelines for Avalanche Professionals in the U.S.* American Avalanche Association (No. ISBN-13: 978-0-9760118-1-1). Pagosa Springs, Victor, United States of America.
- Gubler, H., 1987. Measurements and modelling of snow avalanche speeds, in: *Proceedings of the Davos Symposium*. Presented at the Avalanche Formation, Movement and Effects, Davos.
- 630 Guimbert, S., 2004. Structure and performance of the Afghan economy. World, Washington D.C, United States.
- Hafner, E.D., Techel, F., Leinss, S., Bühler, Y., 2021. Mapping avalanches with satellites – evaluation of performance and completeness. *The Cryosphere* 15, 983–1004. <https://doi.org/10.5194/tc-15-983-2021>
- Hammond, J.C., Saavedra, F.A., Kampf, S.K., 2018. Global snow zone maps and trends in snow persistence 2001–2016. *International Journal of Climatology* 38, 4369–4383. <https://doi.org/10.1002/joc.5674>
- 635 Islamic Republic of Afghanistan Governmental Website, 2021. Badakhshan [WWW Document]. English. URL <https://president.gov.af/en/badakhshan/> (accessed 8.31.21).
- Karas, A., Karbou, F., Giffard-Roisin, S., Durand, P., Eckert, N., 2021. Automatic Color Detection-Based Method Applied to Sentinel-1 SAR Images for Snow Avalanche Debris Monitoring. *IEEE Transactions on Geoscience and Remote Sensing* 60, 1–17. <https://doi.org/10.1109/TGRS.2021.3131853>
- 640 Keylock, C.J., McClung, D.M., Magnusson, M.M., 1999. Avalanche risk mapping by simulation. *Journal of Glaciology* 303–314.
- Kravtsova, V.I., 1990. Snow Cover Mapping of Afghanistan’s Mountains with Space Imagery. *Mapping Sciences and Remote Sensing* 27, 295–302. <https://doi.org/10.1080/07493878.1990.10641815>

- 645 Leinss, S., Wicki, R., Holenstein, S., Baffelli, S., Bühler, Y., 2020. Snow avalanche detection and mapping in multitemporal and multiorbital radar images from TerraSAR-X and Sentinel-1. *Natural Hazards and Earth System Sciences* 20, 1783–1803. <https://doi.org/10.5194/nhess-20-1783-2020>
- Louge, M.Y., Turnbull, B., Carroll, C., 2012. Volume growth of a powder snow avalanche. *Annals of Glaciology* 53, 57–60. <https://doi.org/10.3189/2012AoG61A030>
- 650 Maggioni, M., Gruber, U., 2009. The influence of topographic parameters on avalanche release dimension and frequency. *Cold Regions Science and Technology, ISSW 2002: International Snow Science Workshop* 37, 407–419. [https://doi.org/10.1016/S0165-232X\(03\)00080-6](https://doi.org/10.1016/S0165-232X(03)00080-6)
- Malnes, E., Eckerstorfer, M., Vickers, H., 2015. First Sentinel-1 detections of avalanche debris. *The Cryosphere Discussions* 9, 1943–1963. <https://doi.org/10.5194/tcd-9-1943-2015>
- 655 Martinez-Vazquez, A., Fortuny-Guasch, J., 2008. A GB-SAR Processor for Snow Avalanche Identification. *IEEE Transactions on Geoscience and Remote Sensing* 46, 3948–3956. <https://doi.org/10.1109/TGRS.2008.2001387>
- Mohanty, A., Hussain, M., Mishra, M., Kattel, D.B., Pal, I., 2019. Exploring community resilience and early warning solution for flash floods, debris flow and landslides in conflict prone villages of Badakhshan, Afghanistan. *International Journal of Disaster Risk Reduction* 33, 5–15. <https://doi.org/10.1016/j.ijdrr.2018.07.012>
- OCHA-United Nations, 2012. Districts Affected by Avalanches - Badakhshan Province 19 Jan. 2012.
- 660 Prokop, A., 2008. Assessing the applicability of terrestrial laser scanning for spatial snow depth measurements. *Cold Regions Science and Technology, Snow avalanche formation and dynamics* 54, 155–163. <https://doi.org/10.1016/j.coldregions.2008.07.002>
- Prokop, A., Schön, P., Singer, F., Pulfer, G., Naaim, M., Thibert, E., 2013. Determining Avalanche Modelling Input Parameters Using Terrestrial Laser Scanning Technology. *International Snow Science Workshop Grenoble – Chamonix Mont-Blanc - October 07-11, 2013* 770–774.
- 665 Schaffhauser, A., Adams, M., Fromm, R., Jörg, P., Luzi, G., Noferini, L., Sailer, R., 2008. Remote sensing based retrieval of snow cover properties. *Cold Regions Science and Technology, Snow avalanche formation and dynamics* 54, 164–175. <https://doi.org/10.1016/j.coldregions.2008.07.007>
- Singh, D.K., Mishra, V.D., Gusain, H.S., Gupta, N., Singh, A.K., 2019. Geo-spatial Modeling for Automated Demarcation of Snow Avalanche Hazard Areas Using Landsat-8 Satellite Images and In Situ Data. *J Indian Soc Remote Sens* 47, 513–526. <https://doi.org/10.1007/s12524-018-00936-w>
- Singh, K.K., Singh, D.K., Thakur, N.K., Dewali, S.K., Negi, H.S., Snehamani, Mishra, V.D., 2020. Detection and mapping of snow avalanche debris from Western Himalaya, India using remote sensing satellite images. *Geocarto International* 0, 1–19. <https://doi.org/10.1080/10106049.2020.1762762>
- 675 Smith, W.D., Dunning, S.A., Brough, S., Ross, N., Telling, J., 2020. GERALDINE (Google Earth Engine supRaglAcialL Debris INput dETector): a new tool for identifying and monitoring supraglacial landslide inputs. *Earth Surface Dynamics* 8, 1053–1065. <https://doi.org/10.5194/esurf-8-1053-2020>
- Tompkin, C., Leinss, S., 2021. Backscatter Characteristics of Snow Avalanches for Mapping With Local Resolution Weighting. *IEEE Journal of Selected Topics in Applied Earth Observations and Remote Sensing* 14, 4452–4464. <https://doi.org/10.1109/JSTARS.2021.3074418>
- 680 USAID, 2021. Afghanistan Avalanches [WWW Document]. URL <http://afghanistanavalanches.org/> (accessed 6.30.21).
- Vickers, H., Eckerstorfer, M., Malnes, E., Larsen, Y., Hindberg, H., 2016. A method for automated snow avalanche debris detection through use of synthetic aperture radar (SAR) imaging. *Earth and Space Science* 3, 446–462. <https://doi.org/10.1002/2016EA000168>
- 685 World Bank, 2017. Climate in Crisis: How Risk Information Can Build Resilience in Afghanistan [WWW Document]. URL <https://blogs.worldbank.org/endpovertyinsouthasia/climate-crisis-how-risk-information-can-build-resilience-afghanistan> (accessed 6.30.21).
- Yang, J., Li, C., Li, L., Ding, J., Zhang, R., Han, T., Liu, Y., 2020. Automatic Detection of Regional Snow Avalanches with Scattering and Interference of C-band SAR Data. *Remote Sensing* 12, 2781. <https://doi.org/10.3390/rs12172781>
- 690 Yariyan, P., Avand, M., Abbaspour, R.A., Karami, M., Tiefenbacher, J.P., 2020. GIS-based spatial modeling of snow avalanches using four novel ensemble models. *Science of The Total Environment* 745, 141008. <https://doi.org/10.1016/j.scitotenv.2020.141008>

Zhang, J., Gurung, D.R., Liu, R., Murthy, M.S.R., Su, F., 2015. Abe Berek landslide and landslide susceptibility assessment in Badakhshan Province, Afghanistan. *Landslides* 12, 597–609. <https://doi.org/10.1007/s10346-015-0558-5>

695